Available online at www.sciencedirect.com
SCIENCE DIRECT®
International Journal of Heat and Fluid Flow 24 (2003) 562–571
International Journal of HEAT AND FLUID FLOW
www.elsevier.com/locate/ijhff

Large eddy simulation of a forward–backward facing step for acoustic source identification

Y. Addad [a], D. Laurence [a,b,*], C. Talotte [c], M.C. Jacob [d]

[a] UMIST, MAME Department, Thermo-Fluids Division, P.O. Box 88, Manchester M60 1QD, UK
[b] Electricité de France R&D, MFTT, 6 Quai Watier, F-78400 Chatou, France
[c] Societé Nationale des Chemins de Fer Français, F-7508 Paris, France
[d] UMR CNRS 5509, Ecole Centrale de Lyon, F-69130 Ecully, France

Received 15 December 2002; accepted 23 March 2003

Abstract

The feasibility of using a commercial CFD code for large eddy simulation (LES) is investigated. A first test on homogeneous turbulence decay allows a fine-tuning of the eddy viscosity with respect to the numerical features of the code. Then, a flow over forward–backward facing step at Reynolds number $Re_h = 1.7 \times 10^5$ is computed. The results found show good agreement with the new LDA data of Leclercq et al. [Forward backward facing step pair: aerodynamic flow, wall pressure and acoustic characterization. AIAA-2001-2249]. The acoustic source term, recorded from the LES and to be fed into a following acoustic propagation simulation, is found to be largest in the separation from the forward step. The source terms structures are similar to the vortical structures generated at the front edge of the obstacle and advected downstream. Structures generated from the backward step rapidly break down into smaller scale structures due to the background turbulence.

Keywords: LES; Finite volume method; Separated flows; Bluff body aerodynamics; Acoustics

1. Introduction

Computational fluid dynamics (CFD) is now a common design tool for road vehicles. Powerful and lower cost computers enable parametric studies for improving performance and safety, but the next challenging issue that can lead to significant commercial advantages is comfort of passengers and nuisance reductions for communities nearby roads and rail tracks. With this objective, SNCF (French trains), PSA (Peugeot-Citroen), EDF (Electricité de France) and ECL (Ecole Centrale de Lyon) embarked on a project aiming at numerical prediction of noise (PREDIT 2.2), supported by the French state.

Aerodynamic noise is generated by turbulent structures, but the acoustic energy radiated is a very small fraction of the total flow energy, or even of the turbulent kinetic energy. The non-linear nature of turbulence being so different from that of propagation, hybrid methods are commonly used whereby the flow features and turbulence are computed on the one hand, then introduced as a transporting media and source terms, in a separate acoustic calculation. Some groups, including ECL (Gloerfelt et al., 2001) have resorted to a direct simulation of both phenomena, but this approach is based on high order schemes which cannot be easily extended to industrial geometries. In the present hybrid approach, the linearized Euler equations (LEE) are used for the propagation of noise. The LEE consist of propagation equations for velocity, density and pressure fluctuations, where all non-linear terms are excluded with the notable exception of a source term $S_i = -u'_j \partial u'_i/\partial x_j - \overline{u_j \partial u_i/\partial x_j}$. This term is a fluctuation and as such must be "reconstructed" when a RANS model is used to compute the aerodynamic flow, for instance by the Stochastic Noise Generation and Radiation (SNGR) model (Longatte et al., 1998). Alternatively as in the present project, this source term is evaluated from the instantaneous flowfields of a large eddy simulation (LES). A similar method was successfully applied by Kato et al. (2000) to the flow

* Corresponding author. Tel.: +44-161-200-3704; fax: +44-161-200-3723.
E-mail address: dominique.laurence@umist.ac.uk (D. Laurence).

0142-727X/03/$ - see front matter © 2003 Published by Elsevier Science Inc.
doi:10.1016/S0142-727X(03)00050-X

around an insulator, for a high-speed train also. However, the far-field sound was in this case computed from the instantaneous surface pressure on the insulator. Using the LES + LEE approach, the acoustic power spectrum was successfully predicted for the case of a duct flow obstructed by a 2D diaphragm (Crouzet et al., 2002), and the finite element LES code N3S (Rollet-Miet et al., 1999) was accurate in generating the acoustic source term. The second test case of the PREDIT project, presented hereafter, is a forward backward facing step. A first LES calculation performed by Lazure (2000) was based on the N3S-LES code. The tetrahedral FE mesh was not warranted for this rectangular geometry, nor was it ideal for the interpolation of the source terms onto the Cartesian mesh used for the acoustic propagation calculation. A second simulation was thus undertaken, at the same time evaluating the LES capabilities of the commercial code, Star-CD, commonly used by SNCF.

2. Numerical method

The Star-CD code uses the conservative finite volume method, and an unstructured collocated grid is used to store velocities and scalars at cell centres. To minimize the truncation errors in the convective term of the filtered equations, the central second order-differencing scheme is used preferentially to the default upwind or QUICK scheme. To ensure stability, the so-called centred scheme uses in fact an upwind scheme on the implicit part of the equations (i.e. evaluated at time step $n+1$), and on the right hand side the difference between the centred and upwind convection term (i.e. explicitly, at time step n). The diffusion terms are treated using the second order Crank–Nicholson scheme. The PISO algorithm ensures the coupling between the velocity and the quasi-pressure. The global scheme is thus second order in space but formally first order in time. Thanks to this trade-off the scheme is very stable (an understandably mandatory condition for a commercial code) even when CFL numbers higher than 2.5 appear on the front corner of the forward step.

The Smagorinsky model for the eddy viscosity is: $\nu_T = (C_s D\bar{\Delta})^2(2\overline{S}_{ij}\overline{S}_{ij})^{1/2}$ in which $\bar{\Delta}$ is the mean radius of a grid cell (computed as the cubic root of its volume), D is the Van Driest (1956) near-wall damping function $D = 1 - \exp(-y^+/A^+)$ and $\overline{S}_{ij}$ is the filtered strain rate tensor. The value of the coefficient C_s is defined further down. The present model is based on rather crude assumptions. However, it was shown to give satisfying results in similar studies of flow over bluff bodies when sufficient space resolution is used, as reported by Werner and Wengle (1989) and Yang and Ferziger (1993). This is due to the fact that the flow is dominated by large-scale unsteady structures. Furthermore, the simplicity in the physical aspect of the model makes it easier to identify the numerical filter introduced. Thus, it serves well the intention of the present work to test the capability of using commercial code in a LES calculation.

3. Determination of the constant C_s

Prior to any LES application of a commercial or industrial code, its performance on homogeneous isotropic turbulence (HIT) should be established. As shown by Rollet-Miet et al. (1999), this can be extremely informative. Moreover, the quality of the predicted acoustic power spectrum is obviously highly dependent on the quality of the source term spectrum. As no such information was available for Star-CD, Y. Addad first undertook the LES simulation of the classical HIT test, using the Comte-Bellot and Corrsin (1971) (CBC) grid turbulence decay experiment.

A computational domain (a cubic box with periodic boundary conditions in all three coordinate directions) is discretized, using a uniform Cartesian grid with 32^3 control volumes. The length of the domain $L = 0.628$ m is chosen such that the cutoff wave number K_c is situated within the inertial zone. The initial field is constructed to fit the energy spectrum of the experiment at the station $tU_0/M = 42$ (where U_0 is the flow velocity and M is the mesh size in the experiment) and satisfying incompressibility and the appropriate skewness value of -0.4. Then, comparisons are made with the filtered spectrum at the station $tU_0/M = 98$ after a simulated time of 0.282 s.

The Smagorinsky model is based on equilibrium assumptions well verified in HIT, and the value of the constant C_s can be derived, laying within the range of 0.18–0.22 as found in the literature (see for example, Fureby et al. (1997), Canuto and Cheng (1997), and Sagaut (2001)). Thus any discrepancies found in the results can be attributed to numerical and not modeling issues.

A wider range of values is found in the literature, possibly to compensate numerical diffusion of each specific code. In HIT the total dissipation ε, can be defined from the decay of kinetic energy, then split in two parts:

$$\mathrm{d}k/\mathrm{d}t = -\varepsilon = -(\varepsilon_{\mathrm{mod}} + \varepsilon_{\mathrm{num}}) \tag{1}$$

$\varepsilon_{\mathrm{mod}}$ is the physical dissipation due to the SGS model, and $\varepsilon_{\mathrm{num}}$ is the one presumed to be introduced by the numerical dissipation. If the simulation is run with neither any SGS model nor molecular viscosity, then the first term in Eq. (1) vanishes. Such an inviscid HIT simulation was run and the Star-CD code reproduced the transition from the Kolmogorov $n = -5/3$ spectrum to the expected $n = +2$ power law of the spectrum, without any stability problems, but the total energy

decayed enabling the identification of ε_{num}. However this puts a huge emphasis on the small scales and it is better to evaluate ε_{num} in the presence of a $n = -5/3$ spectrum which corresponds to real applications. ε_{mod} is easily evaluated, then ε_{num} is obtained by the balance of (1).

If the numerical error is assumed to be proportional to velocity gradients (as in first order schemes), the resulting numerical dissipation can be written as a function of a numerical turbulent viscosity and the strain rate of the large resolved eddies:

$$\varepsilon_{num} = -2\nu_{Tnum} S_{ij} S_{ij} \tag{2}$$

Assuming that the turbulent numerical viscosity ν_{Tnum} is varying similarly to the physical one:

$$\nu_{Tnum} = (C_{snum}\bar{\Delta})^2 (2\overline{S}_{ij}\overline{S}_{ij})^{1/2} \tag{3}$$

where the "numerical Smagorinsky constant" C_{snum} can be subtracted from the theoretical one to give the convenient optimal constant $C_{s\ opt}$ for the present code.

The variation of the numerical constant as a function of time in the CBC simulation is presented in Fig. 1. The numerical constant C_{snum} is stabilized after a long computation time; it has been evaluated around the value of 0.054. Note that the fact that C_{snum} shows moderate variations while the strain rate decays significantly is a confirmation of the scaling used in Eq. (3). Fig. 2 illustrates the spectrum obtained using the resulting constant $C_{s\ opt} = 0.126$ and the one with the theoretical value of 0.18 in comparison to the experiments. As it can be seen clearly, results are improved. Such a compensation for numerical diffusion could probably be obtained by a using a Dynamic Model as shown by Rollet-Miet et al. (1999), but would not enable for instance a fine channel flow LES including the viscous sublayer where the Smagorinsky constant needs to decrease to zero. However, the code is suitable for bluff body flows, as in the present case, where the turbulent resolved scales are mainly generated by separated shear layers.

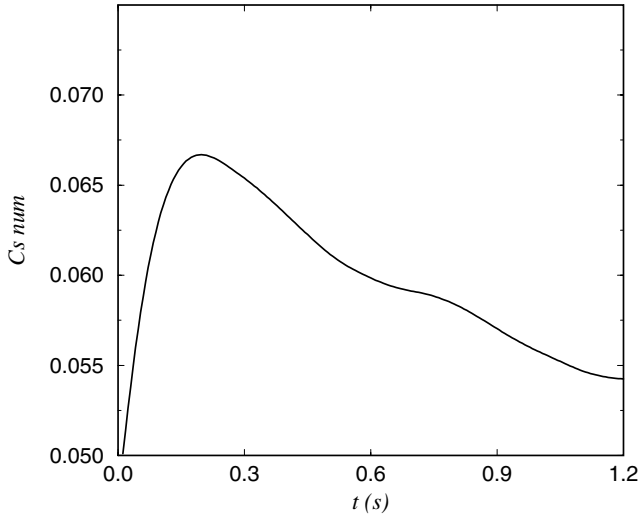

Fig. 1. The numerical Smagorinsky constant variation as function of the simulation time (simulation without viscosity and without SGS model).

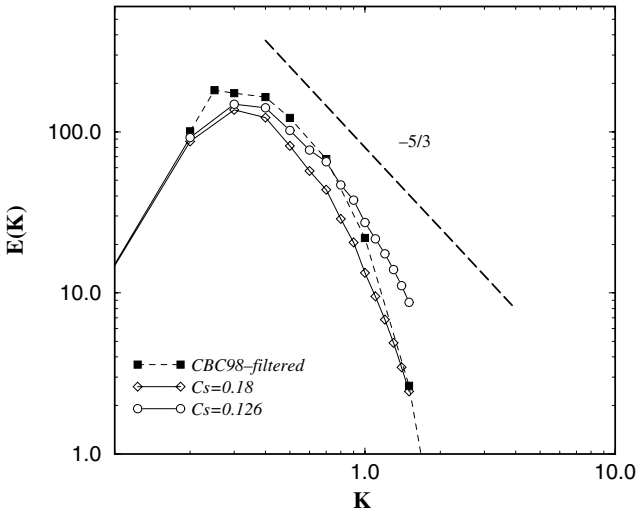

Fig. 2. Energy spectra obtained with theoretical $C_s = 0.18$ and the estimated one 0.126.

It is well known that the value obtained from the energy decay simulations has to be further decreased by a factor of about 2–3 for channel flow simulations, see Piomelli et al. (1988) and Germano (1991). Based on the analysis described above and the observations of previous authors, a value of $C_s = 0.059$ was chosen in the forward–backward step simulation.

4. The forward–backward facing step

The case selected in the present study is a flow over a forward–backward facing step, of height $h = 50$ mm and $l = 10h$ long. The external flow velocity is 50 m/s resulting in Reynolds number $Re_h = 1.7 \times 10^5$ (based on the external velocity and the obstacle height). The upstream boundary layer thickness reported in Leclercq et al. for the LDA measurements was about $0.7h$.

The geometric parameters of the present application are presented in Fig. 3. The domain height is $10h$, the spanwise width of the domain equals $2h$. The inlet and outlet are located at $x = -5h$ and $35h$, respectively, and the step is placed between 0 and $10h$.

A previous LES simulation, Lazure (2000), using the finite element LES code developed by Rollet-Miet et al. (1999) led to correct turbulent intensities and overall noise generation levels, but the separation bubble was underestimated (compared to the one reported in Leclercq et al. (2001)). This is due to insufficient near-wall grid resolution with tetrahedrons (limited aspect ratio).

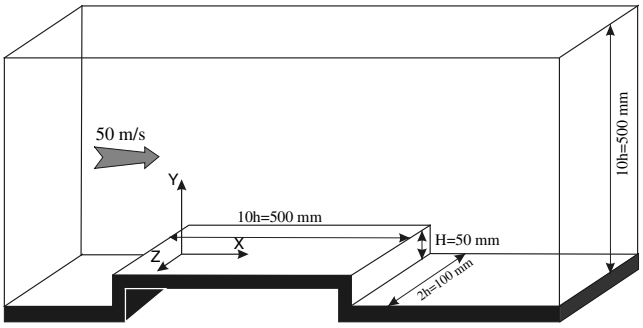

Fig. 3. Physical configuration and the domain dimensions.

In contrast, care was taken in the present study by generating an unstructured grid based on hexahedral cells with four levels of grid refinements with hanging nodes. Within each level the ratios of the cell dimensions are kept constant in the three directions (blocks of cubes) to minimize numerical errors resulting from non-orthogonality and the aspect ratio of cells. The step change in grid sizes can lead to concern relative to theoretical non-commuting errors with non-uniform filter width in space (Ghosal and Moin, 1995), and this location needs to be monitored. On the top of the step, the centre of the control volume adjacent to the wall was placed under $\Delta y^+ = 10$ in the recirculation bubble region. As a consequence, the grid is densely packed around the step and near the wall, with a "hanging nodes" grid expansion in all three directions (see Fig. 4), resulting in total number of control volumes of 260,000. A Cartesian mesh with the same near-wall resolution would have resulted in a total of 7 million cells, so the use of hanging nodes provides huge savings. Periodic boundary conditions are employed in the homogenous (z) direction; at the wall, the standard logarithmic wall function was imposed, and in the upper limit of the domain symmetric boundary conditions are imposed. The inlet profile imposed was obtained from 1/7 a power law profile, close to the first set of hot wire measurements, with a boundary layer thickness of $\delta = 0.7h$. This value, corresponding to the first measurement campaign using hot wires reported in Leclercq et al., differs from the later LDV measurements showing instead $\delta = 0.5h$, but available after the simulation. The Star-CD code provides random perturbations at the entrance, and an initial test with a fluctuation intensity level of 5% showed that these decayed too rapidly before reaching the step, so the level was set to 10%. The outlet boundary is placed at a far enough downstream position ($35h$) to avoid any perturbations related to outflow boundary condition.

Two simulations were launched in parallel using different initial conditions, one using a high Reynolds k–ε initialisation, with a too short recirculation (LES1), and the other (LES2) using preliminary LES calculation results which had a too long recirculation (due to inappropriate wall function implementation). The two initialisations being quite different, the convergence of the statistics could be more clearly monitored.

The two calculations were continued for a number of iterations covering two sweeps through the domain ($t = 2 \times 35h/U_{\text{ref}}$). Only then was the storage of instantaneous fields for the statistical averages started, and lasting for a period equivalent to 6 times the same characteristic time $35h/U_{\text{ref}}$. The CPU time needed, on the Origin IRIX-2000 at UMIST, to run the calculations was about 60 days. The averaging was then performed in the homogeneous directions and in time.

5. Results and discussion

The flow develops three recirculation zones around the step. Fig. 5 shows streamlines obtained from the averaged field where the three distinct recirculation zones are observed. The separation and reattachment points of the first bubble in the region before the forward step are in good agreement with the experimental data of Leclercq et al. (2001) and Moss and Baker (1980). In the experiments, the flow detaches at 0.8–1.5h before the step to reattach on the vertical wall at 0.6–0.65h. The corresponding values in the present calculation are 1.2h and 0.6h respectively. The second recirculation zone predicted by the present calculations ends at 4.7h, and the same value is reported by Moss et al. (1980), while in Leclercq et al. (2001) a rather smaller

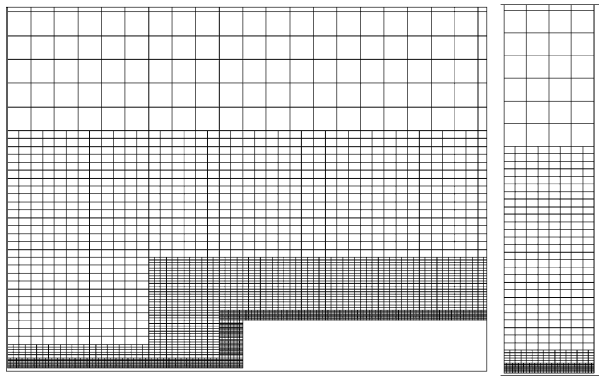

Fig. 4. A small section of the grid showing the four levels of refinement in all three directions.

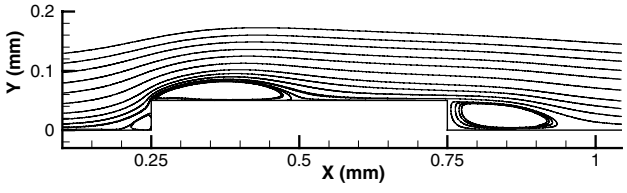

Fig. 5. Streamlines obtained from the averaged velocities of the LES calculation.

distance of about $3.2h$ is observed. The flow separates again at the edge of the backward step and reattaches at about $4h$ in the LES computations. The experimental value found in Leclercq et al. (2001) is about $3.5h$.

Profiles of averaged velocities and turbulent fluctuations in the streamwise (U, u'), and normal (V, v') directions, compared with the LDA measurements (EXP.) at selected streamwise locations are presented in Figs. 6–9. Solid side-walls are used in the recent measurement campaign with LDA, instead of the permeable ones used with the hot wires campaign to allow simultaneous acoustic measurements, and reported in Leclercq et al. (2001). Indeed these gauze walls introduced some lateral mass flow rate leakage in front of the obstacle, so only the new LDA data is used for comparison with the LES. All the variables presented here are normalised by the free-stream velocity at the inlet U_{ref}. The streamwise and normal velocities show good agreement with the LDA data. The LES profiles obtained (LES1 and LES2) overlap and thus assess the convergence of the simulations. The present simulations converge closer to the Moss and Baker (1980) data presented here for a reference, but unfortunately that experiment only featured a forward step. The actual differences are maybe due to the small difference in the ratio between the boundary thickness and the step height in the inlet profile imposed in the present simulations, or the gauze wall still imposed on the roof of the channel in the LDA campaign.

The rms values of fluctuations on the other hand, show a moderate convergence due to the white noise imposed at the inlet. The rather jagged profiles remain unchanged when increasing the integration time, and LES1 and LES2 do not converge at the entrance. This means that the random process is too dependent on the seeding, and does not de-correlate over time. However one sees better convergence and realistic profiles near the obstacle as new turbulent structures are generated by the forward step. Further downstream, at $x/h = 11$ and 13 the agreement with the experiment is quite satisfactory, and the fact that LES1 and LES2 overlap shows that statistics are converged (at earlier times and due to the very different initialisations, LES1 showed very little fluctuations while LES2 was overestimating them). At $x/h = 11$, a peak in rms fluctuation is clearly seen around $y = 1h$, resulting from the shear layer of the backward step and superimposed to the high background turbulence convected from the forward step separation. The apparent discrepancy at $x/h = 5$ is due to the shorter recirculation bubble in the LDA experiment where the flow has already reattached, and is consistent with the mean velocity profiles shown in Fig. 6, $x/h = 5$, where the LES agrees with the Moss and Baker data.

Overall agreement is thus quite satisfactory, and if we accept that the differences on the forward step are due boundary conditions not replicating accurately

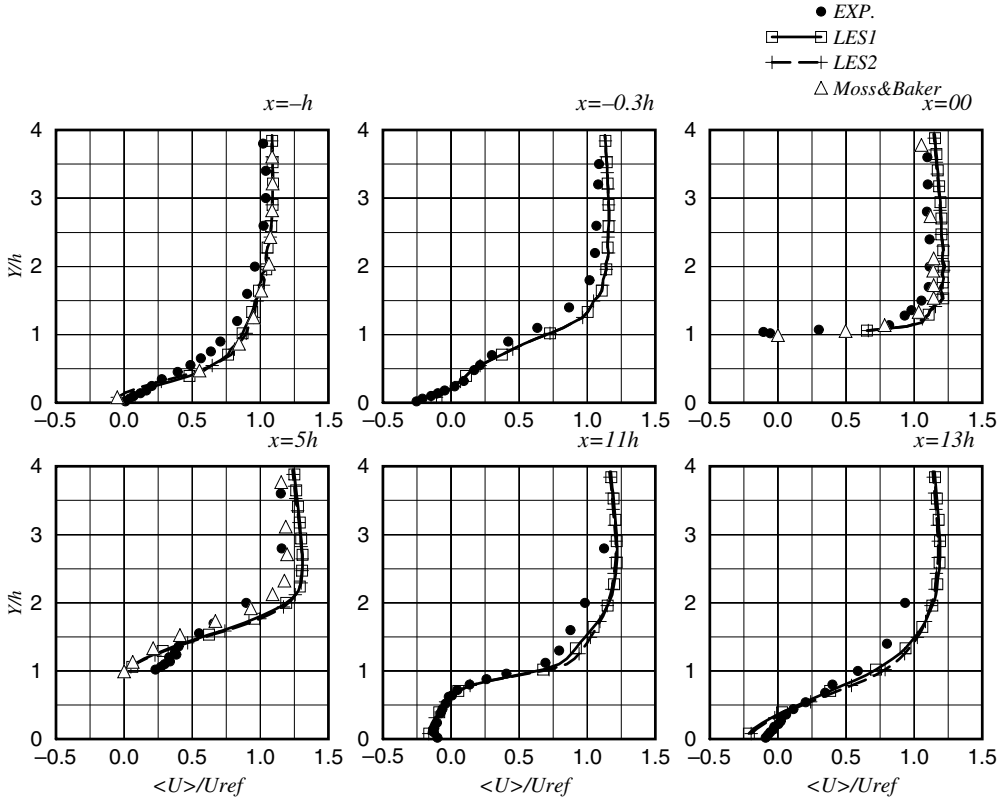

Fig. 6. Streamwise velocity component U normalised by the inlet free-stream value.

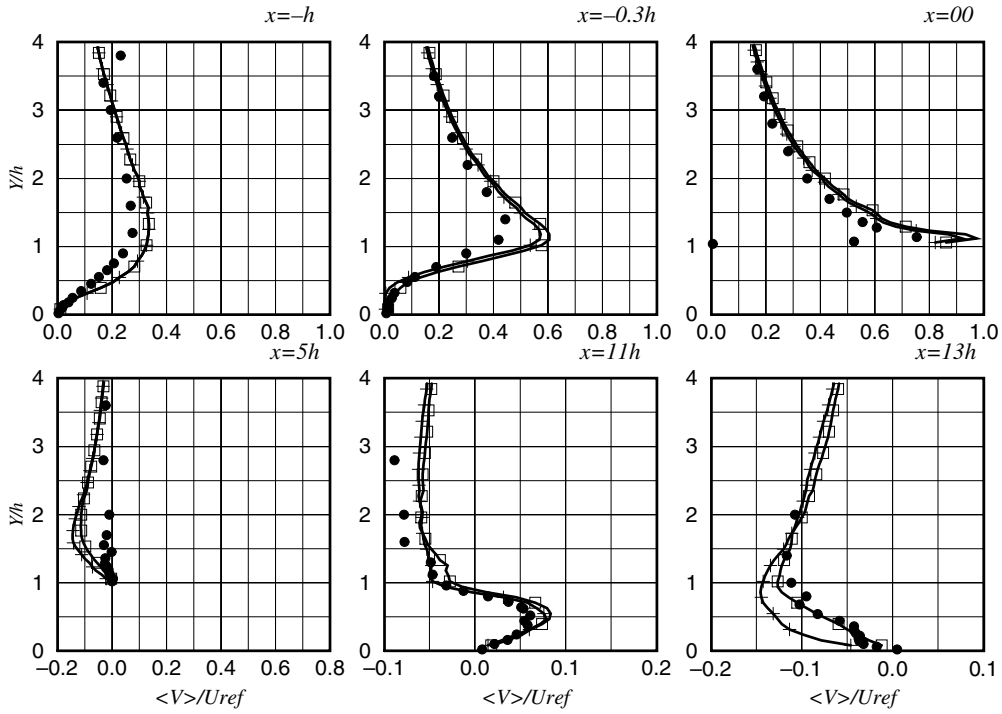

Fig. 7. Profiles of the normal velocity component V normalised by the inlet free-stream velocity.

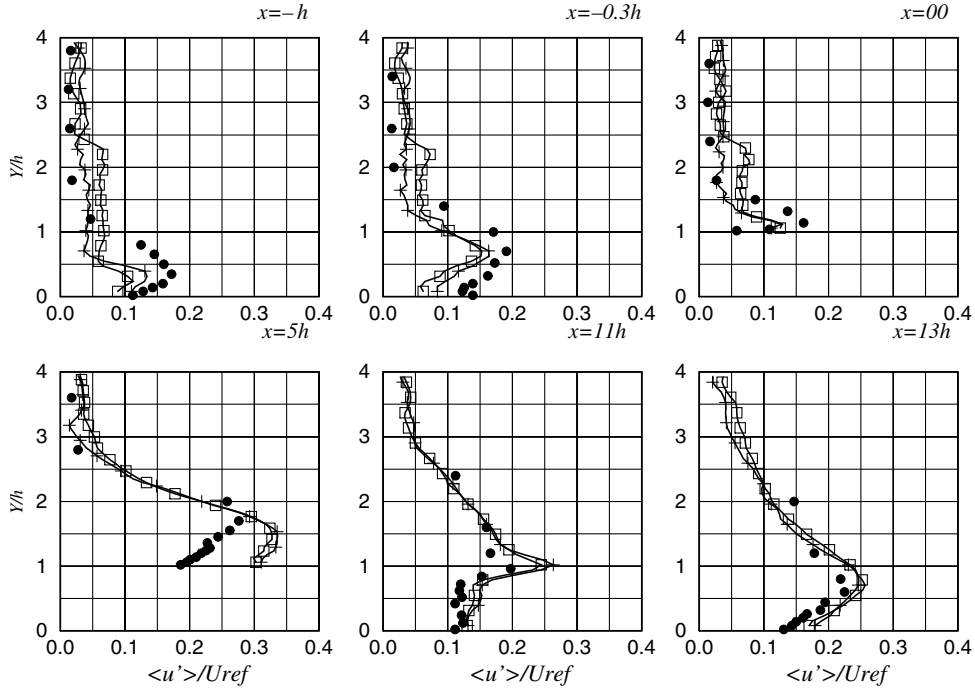

Fig. 8. The streamwise turbulent fluctuation u' normalised by the inlet free-stream velocity.

experimental conditions, then one can conclude that the commercial code is quite suitable for LES applications to bluff bodies, with the provision that inlet turbulence generation needs to be re-examined. It should be noted also that no trace can be seen, on either mean or rms profiles, of the jump in mesh size at location of hanging nodes. A satisfying feature which needed to be verified.

Fig. 10 shows iso-values of the modulus of the vorticity vector (normalised by the inlet free-stream velocity and the step height) with a significant spanwise

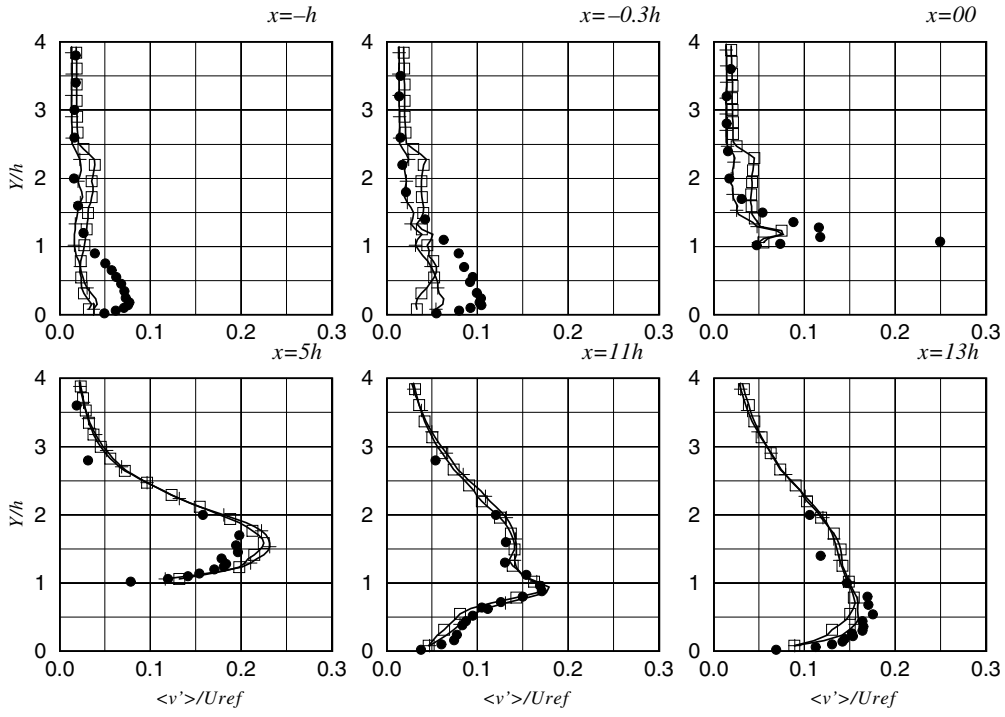

Fig. 9. Profiles of the normal turbulent fluctuation v' normalised by the inlet free-stream velocity.

correlation, especially in the shear layer detaching from the front step. It is mainly the spanwise vorticity component ω_z that carries this correlation, corresponding to vortex shedding from the front corner of the box. The width of the domain of $2h$ seems just about large enough, but this parameter should be tested. These relatively large coherent structures, of the order of h, are seen to persist as they are convected downstream. Near the flow reattachment region these structures break down to small ones due to the three dimensional effects in this region. Smaller structures are generated in the backward step region due to the free shear flow behaviour in this region. Similarly to the Leclercq et al. observations, the flow in this region differs from the classical single backward facing step and exhibits a 50% reduction of the length of the recirculation, due to the incoming perturbations inducing intense mixing effects.

The normalised acoustic source terms S_x and $|S|$ are also shown in Fig. 10. First observations show that the source term structures are generated and convected in the same manner as the vortical structures. The spanwise vortices generate strong streamwise accelerations reflected in S_x, but this spanwise correlation is less than that of ω_z. As noted by Leclercq et al., the backward step is a significantly smaller source of noise, which can only be seen when a lower threshold is plotted. The high level of ambient turbulence probably limits shedding of coherent vortices. However this backward step generates turbulence levels just as high as the forward one, as rms profiles have shown, and this could be a modelling problem when attempting to generate synthetic noise sources using only data from RANS calculations.

To obtain the far-field noise, the linearized Euler equations:

$$\frac{\partial p_a}{\partial t} + \overline{u_j}\frac{\partial p_a}{\partial x_j} + u_{ja}\frac{\partial \overline{p_0}}{\partial x_j} + \gamma\overline{p_0}\frac{\partial u_{ja}}{\partial x_j} + \gamma p_a\frac{\partial \overline{u_j}}{\partial x_j} = 0$$

$$\frac{\partial u_{ai}}{\partial t} + \overline{u_j}\frac{\partial u_{ai}}{\partial x_j} + u_{ja}\frac{\partial \overline{u_i}}{\partial x_j} + \frac{1}{\rho_0}\frac{\partial p_a}{\partial x_i} - \frac{p_a}{\rho_0^2 c_0^2}\frac{\partial \overline{p_0}}{\partial x_i} = S_i$$

are solved using the mean velocities and pressures obtained from the LES, and the source term, $S_i = -u_j'\partial u_i'/\partial x_j - \overline{u_j\partial u_i/\partial x_j}$, is introduced at each time step using the instantaneous velocity field recorded during the LES. A snapshot of the acoustic pressure is shown in Fig. 11.

This two-step method entails large data storage and manipulation which could have been avoided by performing the acoustic calculation in parallel with the LES, but the LEE calculation was performed by separately by Crouzet and Lafon at EDF as the LEE code was not available at UMIST.

The acoustic power of the far-field noise was however overestimated by several dB. On the other hand the acoustic power of the second "PREDIT" test case, a diaphragm in a duct, was well simulated by the same LES-LEE method (Crouzet et al., 2002), and this may be due again to the porous walls used on the sides and top of the duct. Indeed, when the glass side-walls used with LDA were replaced by gauze for the acoustic measurements, HW measurements indicated a maximum velocity

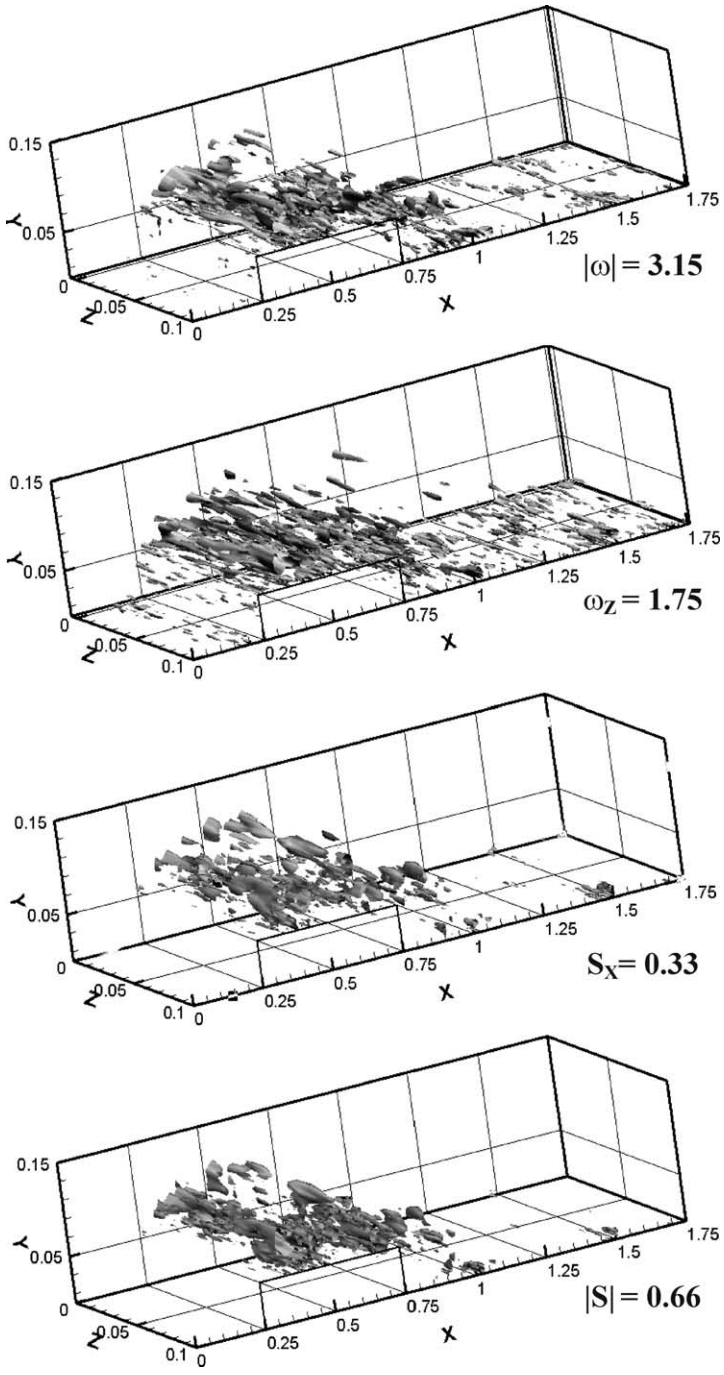

Fig. 10. Iso-values of the vorticity and the acoustic source term.

above the step about 5% lower than the same measurements with LDA. In fact the flow is closer to that over a 3D box whereas the LES with lateral periodicity conditions represents a wide 2D obstacle.

6. Conclusion

The calibration of the classical Smagorinsky subgrid model constant was carried out using the homogeneous turbulence decay and taking in account the numerical dissipation identified in the commercial code. Then, results from two large eddy simulations of a flow over forward–backward facing step at Reynolds number $Re = 1.7 \times 10^5$ are presented. Running two independent calculations simultaneously, starting from very different initial conditions was found useful in monitoring statistical convergence. It also has enabled to identify some defaults in the inlet turbulence generation process, which needs to be re-examined. Apart from this, the

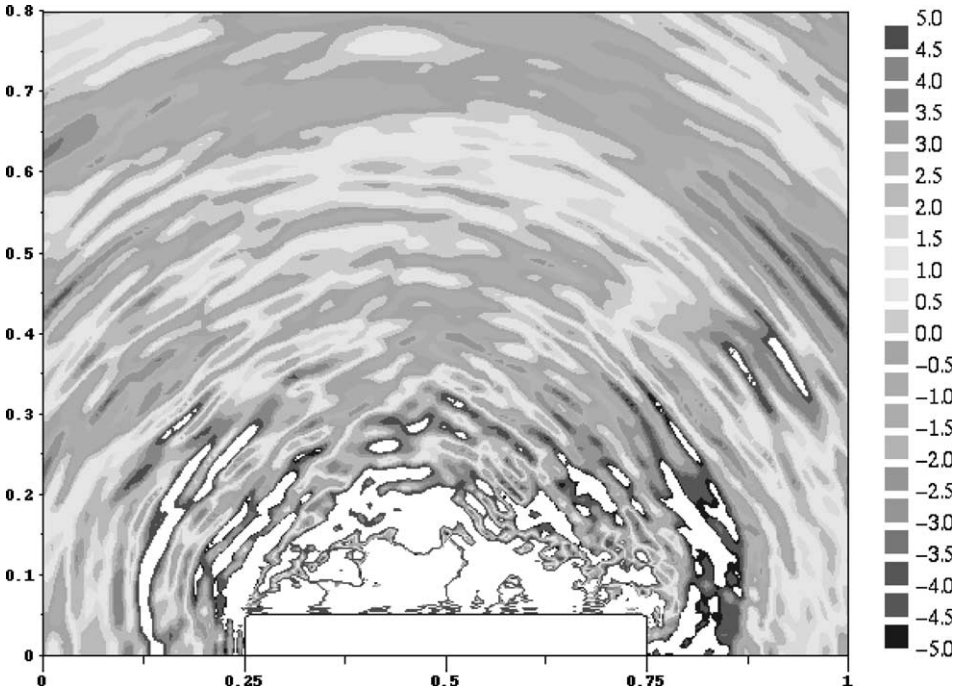

Fig. 11. Iso-values of instantaneous acoustic pressure obtained from the LEE (from Crouzet).

commercial code is found well suitable for the LES of bluff bodies, and the extensive use of hanging nodes resulted in very large savings in cell numbers, without introducing any perturbation. The results obtained are in overall good agreement with the LDA data, except after the front step where they agree better with older data, so this may be due to differences in the experimental conditions. The acoustic source term identification show its relation with the vortices in the free shear layer.

Acknowledgements

C. Talotte and M.C. Jacob gratefully acknowledge support from the PREDIT programme of the French Ministère de l'Education Nationale, de la Recherche et de la Technologie. Y. Addad and D. Laurence gratefully acknowledge support from the Algerian Ministère de l'Enseignement et de la Recherche scientifique, and are thankful to Dr. A. Ghobadian, Dr. R. Clayton (Computational Dynamics Ltd.), S. Benhamadouche, and F. Crouzet (EDF) for assistance and helpful discussions.

References

Canuto, V.M., Cheng, Y., 1997. Determination of the Smagorinsky-Lilly constant Cs. Phys. Fluids 9 (5), 1368–1378.

Comte-Bellot, G., Corrsin, S., 1971. Simple eulerian time correlation of full- and narrow-band velocity signals in grid-generated 'isotropic' turbulence. J. Fluid Mech. 48, 273–337.

Crouzet, F., Lafon, P., Buchal, T., Laurence, D., 2002. Aerodynamic noise prediction in internal flows using LES simulations and Euler equations acoustic modelling. 8th AIAA/CEAS Aero-acoustics Conference, 17–19 June 2002, Colorado.

Fureby, C., Tabor, G., Weller, H.G., Gosman, A.D., 1997. A comparative study of subgrid scale models in homogeneous isotropic turbulence. Phys. Fluids 9 (5), 1416–1429.

Germano, M., 1991. Turbulence: the filtering approach. J. Fluid Mech. 238, 325.

Ghosal, S., Moin, P., 1995. The basic equations for the large eddy simulation of turbulent flows in complex geometry. J. Comput. Phys. 118, 24–37.

Gloerfelt, X., Bailly Ch Juvé, D., 2001. Computation of the noise radiated by a subsonic cavity using direct simulation and acoustic analogy. AIAA paper 2001-2226.

Kato, C., Iida, A., Inadama, S., 2000. Numerical simulation of aerodynamic sound source in the wake of a complex object. AIAA-2000-1942.

Lazure, H., 2000. Calculs acoustiques sur le cas SNCF et premières comparaisons caluls-essais. SNCF Dir. Recherche & Technologies ref. 1T090500A, 09/05/00.

Leclercq, D.J.J., Jacob, M.C., Louistot, A., Talotte, C., 2001. Forward backward facing step pair: aerodynamic flow, wall pressure and acoustic characterization. AIAA-2001-2249.

Longatte, E., Lafon, P., Candel, S., 1998. Computation of noise generation by turbulence in internal flows. AIAA paper 98-2332.

Moss, W.D., Baker, S., 1980. Re-circulating flows associated with two-dimensional steps. Aero Quart., 151–172.

Piomelli, U., Moin, P., Ferziger, J.H., 1988. Model consistency in large eddy simulation of turbulent channel flow. Phys. Fluids 31 (7), 1884, 1891.

Rollet-Miet, P., Laurence, D., Ferziger, J.H., 1999. LES and RANS of turbulent flow in tube bundles. Int. J. Heat Fluid Flow 20 (3), 241–254.

Sagaut, P., 2001. Large Eddy Simulation for Incompressible Flows. Springer-Verlag.

Van Driest, E.R., 1956. On turbulent flow near a wall. J. Aerospace Sci. 23, 1007–1011.

Werner, H., Wengle, H., 1989. Large-eddy simulation of turbulent flow over a square rib in a channel. In: 7th Symposium on Turbulent Shear Flows, Stanford Univ., Stanford, CA, August 21–23.

Yang, K.S., Ferziger, J.H., 1993. Large-eddy simulation of turbulent obstacle flow using a dynamic subgrid-scale model. AIAA J. 31 (8), 1406–1413.